Analyst

PAPER

View Article Online
View Journal | View Issue

Cite this: *Analyst*, 2024, **149**, 2697

The role of cardiolipin and cytochrome *c* in mitochondrial metabolism of cancer cells determined by Raman imaging: *in vitro* study on the brain glioblastoma U-87 MG cell line

Monika Kopeć, *[a,b] Aleksandra Borek-Dorosz,[b] Karolina Jarczewska,[a] Małgorzata Barańska[b] and Halina Abramczyk[a]

In this paper, we present Raman imaging as a non-invasive approach for studying changes in mitochondrial metabolism caused by cardiolipin–cytochrome *c* interactions. We investigated the effect of mitochondrial dysregulation on cardiolipin (CL) and cytochrome *c* (Cyt *c*) interactions for a brain cancer cell line (U-87 MG). Mitochondrial metabolism was monitored by checking the intensities of the Raman bands at 750 cm^{-1}, 1126 cm^{-1}, 1310 cm^{-1}, 1337 cm^{-1}, 1444 cm^{-1} and 1584 cm^{-1}. The presented results indicate that under pathological conditions, the content and redox status of Cyt *c* in mitochondria can be used as a Raman marker to characterize changes in cellular metabolism. This work provides evidence that cardiolipin–cytochrome *c* interactions are crucial for mitochondrial energy homeostasis by controlling the redox status of Cyt *c* in the electron transport chain, switching from disabling Cyt *c* reduction and enabling peroxidase activity. This paper provides experimental support for the hypothesis of how cardiolipin–cytochrome *c* interactions regulate electron transfer in the respiratory chain, apoptosis and mROS production in mitochondria.

Received 3rd January 2024,
Accepted 27th February 2024

DOI: 10.1039/d4an00015c

rsc.li/analyst

Introduction

Cytochrome *c* is a crucial protein that is required to maintain life (respiration) and cell death (apoptosis). The most common function of Cyt *c* is an electron shuttle between complexes **III** and **IV** of mitochondria. Hexa-coordination of heme-iron in native Cyt *c* decreases the occurrence of peroxidase functions. However, the binding of Cyt *c* to anionic phospholipids unfolds the protein and converts it from an electron shuttle into a potent peroxidase. In mitochondria, this peroxidase activity displays remarkable specificity towards CL, causing oxidation and hydrolysis of cardiolipin-OOH.[1]

Removal of a relatively weak ligand, Met(80), changes of the spin-state and structural rearrangements pave the way for opening of the heme catalytic site to small molecules (including H_2O_2 and fatty acid-OOH) to bolster its catalytic activity to levels comparable to those of genuine peroxidases. The peroxidase function of Cyt *c* requires its direct physical interaction with CL. Normally, the regulation of Cyt *c* as a peroxidase is achieved through the very low availability of CL that prevents the formation of cytochrome *c*/cardiolipin complexes. Under pathological conditions, accumulation of cardiolipin occurs which triggers the apoptotic program.[2]

Numerous scientific discoveries, in the field of cell metabolism, suggest that changes in mitochondrial metabolism can be important cancer drivers. Cardiolipin and Cyt *c* can be biomarkers to control the development and progression of cancer.[2–11] It has been reported that the CL–Cyt *c* complex has cytotoxicity for cancer cells.[12]

Cardiolipin is a phospholipid compound which is present in the inner mitochondrial membrane,[13] which includes about 20% of cardiolipins among the total lipid composition.[14,15] For the first time CL was isolated from the beef heart.[16,17] Cardiolipin consists of two phosphatidic acid moieties, which are connected with a glycerol backbone in the center to form a shape of a dimeric structure.[18]

In the last decade, the ability of CL to dysregulate cell metabolism has been studied by numerous researchers.[15,19,20–27,28–30] Cardiolipin can be considered a cancer marker, especially in breast,[2,31,32] thyroid[33,34] and brain[35–37] cancer. The role of CL in MDA-MB-231 cell lines has been studied by S. Hardy *et al.* They demonstrated that a decrease in CL amount and altered mitochondrial function are involved in palmitate-affected cell death.[32] Other researchers

[a]*Lodz University of Technology, Institute of Applied Radiation Chemistry, Laboratory of Laser Molecular Spectroscopy, Wroblewskiego 15, 93-590 Lodz, Poland. E-mail: monika.kopec@p.lodz.pl; Tel: +48426313188*
[b]*Jagiellonian University, Faculty of Chemistry, Gronostajowa 2, 30-387 Krakow, Poland*

used nuclear magnetic resonance to analyze the interaction of doxorubicin with CL. They monitored changes in the membrane bilayer after doxorubicin addition.[38] Another group investigated CL distribution in the intramitochondrial membrane during apoptosis. A study by M.G. Fernandez *et al.* reported that increased production of reactive oxygen species during the apoptosis process could change the distribution of CL.[39]

Monitoring the role of Cyt *c* in cancer detection has been analyzed in numerous successful reports.[2,5,40–47] With Raman microspectroscopy, N. Brazhe *et al.* investigated the redox status of cytochromes in cardiomyocytes. Their experiment shows that the amount of reduced cytochromes in rod-shaped cardiomyocytes decreases under oxidative stress conditions.[48] Another group studied the ability of Raman spectroscopy to detect the apoptosis process mediated by Cyt *c* in the MCF-7 cell line. They determined the concentration of a proapoptotic drug (paclitaxel 100 μM) which triggers the release of Cyt *c* to the cytoplasm.[49] A study by Y. Sun *et al.* shows the role of Cyt *c* in non-small cell lung cancer (NSCLC) by surface enhanced Raman scattering. They successfully used a SERS biosensor for the detection of Cyt *c* in NSCLC.[50] The role of the interaction of Cyt *c* with CL in metabolism was investigated also by Milorey *et al.*,[45] Chertkova *et al.*,[46] Pletneva's group[47,51] and Vladimirov's group.[52,53] The effect of cardiolipin penetration inside cells was studied also by A.V. Birk *et al.* They have shown that the interaction between CL and Cyt *c* is advantageous for keeping Cyt *c* close to the respiratory complexes and preventing its loss from the inter-membrane space.[54] Interactions of Cyt *c* with CL in the mitochondrial membrane by using Raman spectroscopy have been described by J. Kitt *et al.*[55] Another group has studied the interaction of Cyt *c* with CL by using mass spectrometry.[56]

In this paper, we will discuss the role of CL and Cyt *c* in cancer cell metabolism. We will investigate the uptake of CL and Cyt *c* in human cancer brain cells (U-87 MG) by using Raman spectroscopy and Raman imaging. The main goal of this study is to characterise biochemical changes in cells' mitochondrial metabolism and the redox status of Cyt *c* under pathological conditions of cancer. To the best of our knowledge, this is the first paper that provides experimental evidence that cardiolipin–cytochrome *c* interactions control the redox status of Cyt *c* by switching from the electron carrier in the electron transport chain to the peroxidase activity.

Materials and methods

Chemical compounds

Cardiolipin solution from bovine heart (C1649) and Cytochrome *c* from equine heart (C7752) were purchased from MERCK.

Raman spectroscopy

Raman spectra and images presented in this manuscript were recorded using a confocal Raman microscope (WITec alpha 300 RSA+ (Ulm, Germany)) equipped with a 50 μm core diameter fiber ultra-high throughput spectrometer (UHTS) and a CCD camera (Andor Newton DU970-UVB-353). For measurements, we used a 532 nm excitation laser beam and Nikon objective with a magnification of 40× and a numerical aperture (NA = 1.0) intended for cell measurements performed by immersion in PBS (phosphate buffered saline, Gibco no. 10010023). The average laser excitation power used during analysis was 10 mW and 0.5 s integration time for the fingerprint region and 0.3 s for the high-frequency region have been used. The collected Raman spectra were preprocessed using the WITec Control/Project Four 4.1 package (removal of cosmic rays, and smoothing and background corrections). To analyze the Raman imaging data a cluster analysis method was used. Cluster analysis is a procedure of analysis that allows us to group the Raman spectra into groups called a cluster. Each of the clusters (the Raman spectra) must be as similar as possible in contrast to the Raman spectra belonging to another group. The separation of n observations (x) into k ($k \leq n$) clusters S should be done to minimize the variance (Var) according to the formula:

$$\arg\min_{s} \sum_{i=1}^{k} \sum_{x \in S_i} ||x\mu_i||^2 = \arg\min_{s} \sum_{i=1}^{k} |S_i| \mathrm{Var} S_i$$

where μ_i is the mean of experimental points. In our study, the number of clusters is 7. Each cluster is characterized by specific average Raman spectra, which reflect the inhomogeneous distribution of the samples.[3,5,57]

The stack images were recorded using a confocal Raman microscope (WITec alpha 300 (Ulm, Germany)) located at the Faculty of Chemistry at Jagiellonian University. For measurements, we used a 532 nm excitation laser beam and a 63 × water immersion objective (Zeiss W Plan-Apochromat 63×, NA = 1, Oberkochen, Germany). The average laser excitation power during the analysis was ~30 mW (measured after the beam passed through the objective) and a 0.2 s integration time has been used. Spectral images were collected with a sampling density of 0.5 μm (in z-axis step size was equal to 1.5 μm). The obtained Raman spectra and Raman 3D imaging data were preprocessed using the WITec Control/Project Four 5.1 package (removal of cosmic rays, and smoothing and background corrections).

Before Raman measurements, the growth medium was removed, the cells were fixed with 4% formalin for 10 min and kept in phosphate-buffered saline (PBS, Gibco no. 10010023) during the experiment.

Cell lines

The glioblastoma cell line (U-87 MG; HTB-14™) was purchased from ATCC, the global bioresource center. The glioblastoma cell line was originally obtained from a 44-year-old male patient. For U-87 MG cell line culturing (EMEM; ATCC 30-2003) medium from ATCC was used. To prepare a complete growth medium Fetal Bovine Serum (FBS) was added to a final concentration of 10%.

Cultivation conditions

All experiments presented in this manuscript were conducted using U-87 MG. For cell growth, we used a flat-bottom culture flask with a cell growth surface of 75 cm^2. All cells prepared for analysis were stored in an incubator, which provided ensured access to the conditions necessary for proper culture (37 °C, 5% CO_2, 95% air).

Cell treatment with cardiolipin and cytochrome *c*

All cells prepared for experiments were seeded on CaF_2 windows (Crystran Ltd). Control cells (without any supplementation) for measurement were prepared using the method described below. The medium dedicated to cell growing was removed. Afterwards, the cells were fixed using formalin for 10 min and after that washed twice with PBS. The cells were measured in PBS. Measurements using the Raman method were conducted immediately after the preparation of samples.

All the CL and Cyt *c* solutions used for supplementation were prepared by diluting the pure culture medium dedicated by ATCC to cell lines used in the investigation as a solvent. For the preparation of Cyt *c* solutions with concentrations of 1, 10 and 15 μM we used powdered reagents. For supplementation with CL solution reagents (4.7–5.3 mg mL^{-1} in ethanol, ≥97% (TLC)) were used, from which samples were prepared to finally obtain a solution with concentrations of 1, 10 and 15 μM. The incubation time of the Cyt *c* and CL was 24 h. The solution of Cyt *c* was added simultaneously with CL.

Statistical analysis

All Raman spectra presented in the manuscript were normalized in Origin software by using a model divided by norm.[2] The average Raman spectra and standard deviations (SD) were recorded by using Origin software. To prepare statistically significant differences (labeled *) between the analyzed cell groups the ANOVA (Tukey test, at a significance level of 0.05) in Origin was used.

Results and discussion

First, we analyzed the biochemical composition of unsupplemented U-87 MG cells by Raman imaging. Fig. 1 shows the intracellular structures of U-87 MG cells obtained by 3D Raman imaging along the *z*-axis through a cross-section of the cell. The stack images along the *z*-axis obtained from layers were collected at 1.5 μm steps from top to bottom of the cell. The intracellular structures are visualized by spectral filters: nuclei (DNA/RNA) (780–800 cm^{-1}) and lipid droplets (lipids) (2830–2900 cm^{-1}) (Fig. 1A). For every analyzed layer the average Raman spectrum for cells as a whole is presented in Fig. 1B.

To check the effect caused by CL supplementation we prepared the same analysis for U-87 MG upon incubation with 10 μM. We analyzed the distribution of lipids and nucleic acids in the U-87 MG cells. Fig. 2 presents results upon supplementation with CL at 10 μM.

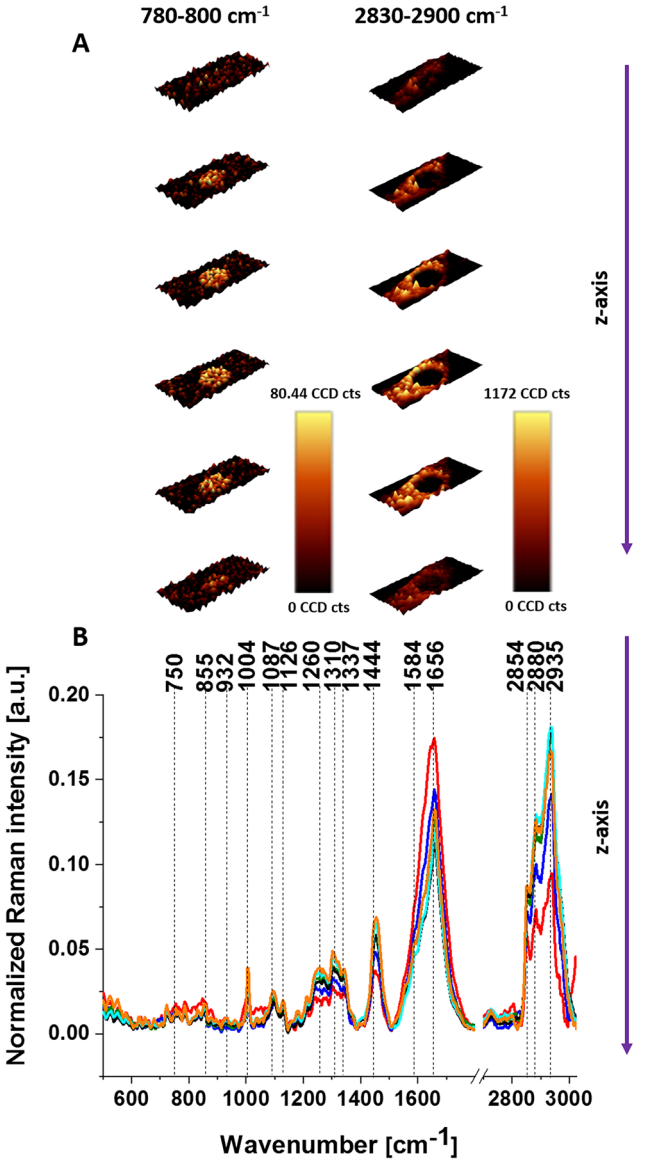

Fig. 1 3D Raman images of glioblastoma (U-87 MG) showing the distribution of nucleic acids (780–800 cm^{-1}) and lipids (2830–2900 cm^{-1}) obtained from each cell layer recorded every 1.5 μm step in the *z*-direction (A) and average Raman spectra for cells as a whole for each layer (B).

Due to the confocality of the Raman microscope, the Raman images present the morphology of the cells and the average Raman spectra for each layer. One can see that at the top images, the laser excites the upper layer of lipid droplets and does not reach the nucleus. Going deeper the Raman images reveal the cross-section through the middle of lipid droplets and nucleus. However, the Raman spectra for each layer represent the average biocomposition of each layer.

One can see that by comparison of Fig. 1 and 2 the lipid droplets are more visible in cells supplemented with 10 μM CL than in cells without supplementation. Such types of measurements are more time-consuming, so we focused on one cell

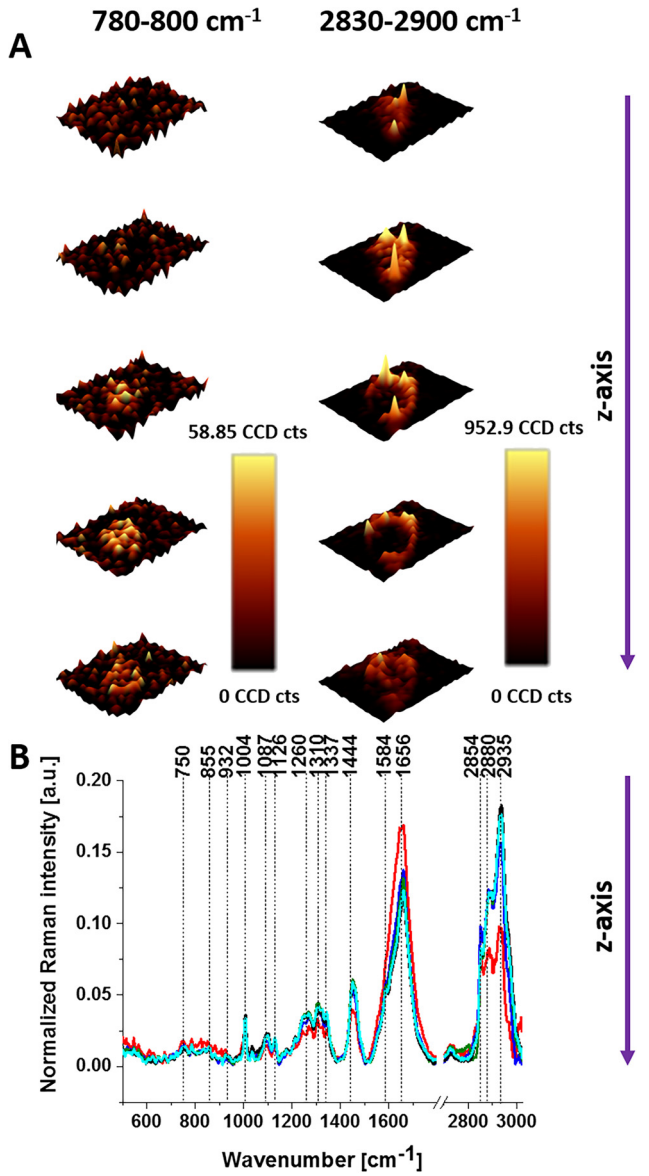

Fig. 2 3D Raman images of glioblastoma (U-87 MG) showing the distribution of nucleic acids (780–800 cm^{-1}) and lipids (2830–2900 cm^{-1}) upon supplementation with 10 μM cardiolipin obtained from layers recorded every 1.5 μm step in the *z*-direction (A) and average Raman spectra for cells as a whole for each layer (B).

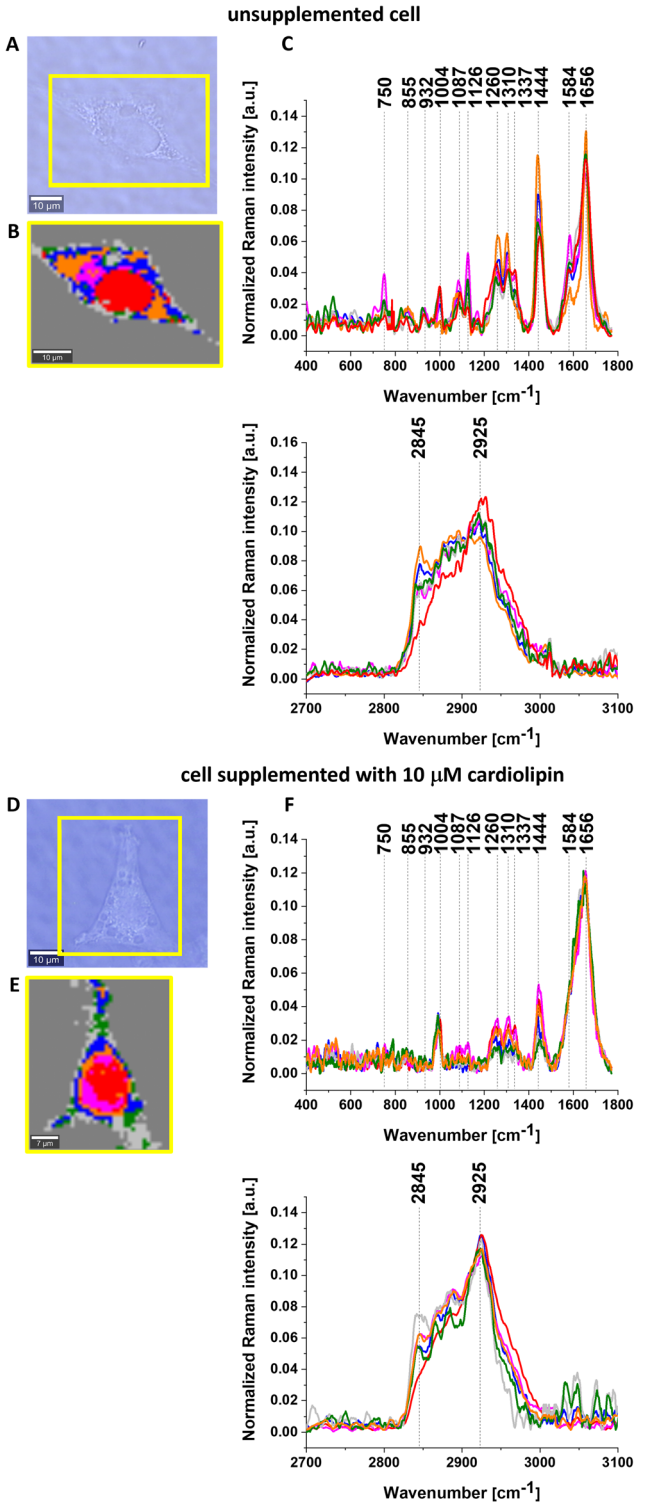

Fig. 3 The microscopy image (A), Raman image (B) and Raman spectra of glioblastoma (C) (U-87 MG) and the microscopy image (D), Raman image (E) and Raman spectra of glioblastoma (F) (U-87 MG) supplemented with 10 μM cardiolipin; Raman images constructed based on cluster analysis method and assigned to: nucleus (red), mitochondria (magenta), lipid regions (blue and orange), cytoplasm (green), cell membrane (light grey) and cell environment (dark grey); colors of the spectra correspond to the colors of the clusters.

layer, which includes all organelles. To learn about the Raman spectra for specific organelles one can use chemometric methods to separate the Raman spectra from different organelles.

Based on the cluster analysis method we can also identify the main cellular organelles, such as the nucleus, mitochondria, lipid regions, cytoplasm and cell membrane. Fig. 3 presents the microscopy image, Raman image and Raman spectra for a typical unsupplemented cell and a cell supplemented with 10 μM CL.

Fig. 3B and E shows the clusters inside a typical brain cancer cell corresponding to the nucleus (red), mitochondria

(magenta), lipid regions (blue and orange), cytoplasm (green), cell membrane (light grey) and the cell environment (dark grey); the colors of the spectra correspond to the colors of the clusters.

A detailed inspection of Fig. 3C and F shows the differences in Raman spectra between the cell without supplementation and the cell incubated with CL. The most significant changes are observed in the Raman signals corresponding to cytochrome *c* and *b*: 750, 1126 and 1584 cm^{-1}.[3,43,58]

To understand the role of the interactions between Cyt *c* with CL in cell metabolism, we monitored cell response by Raman spectroscopy and imaging due to supplementation with Cyt *c* and CL.

In Fig. 4 we show the average Raman spectra of the mitochondria region for the unsupplemented U-87 MG cell line and for seven types of supplementation: (1) 10 μM CL + 1 μM Cyt *c*, (2) 1 μM CL + 1 μM Cyt *c*, (3) 10 μM CL + 10 μM Cyt *c*, (4) 15 μM CL + 1 μM Cyt *c*, (5) 10 μM CL + 15 μM Cyt *c*, (6) 1 μM Cyt *c*, and (7) 10 μM CL.

A detailed inspection of Fig. 4 shows differences in average Raman spectra between the U-87 MG cell (without supplementation) and the cell incubated with CL and Cyt *c*. The most significant changes are observed in the Raman signals corresponding to the vibrations of cytochrome *c* and *b*: 750, 1126, and the vibrations of cytochrome *c*, 1584 cm^{-1}.[2,4,5] The results in Fig. 4 demonstrate that the vibrations of Cyt *c* are sensitive to its interactions with CL. Electrostatic forces are some of the major factors that govern cytochrome *c*–cardiolipin interactions. Positively charged Cyt *c* molecules (an isoelectric point is near pH 10 and the net charge is +8*e* at neutral pH) are strongly attracted to the negatively charged headgroups of anionic lipids including CL.[1] Fig. 4 shows that U-87 MG cancer cells without supplementation (dark grey line) can be distinguished from the U-87 MG cells supplemented with CL and

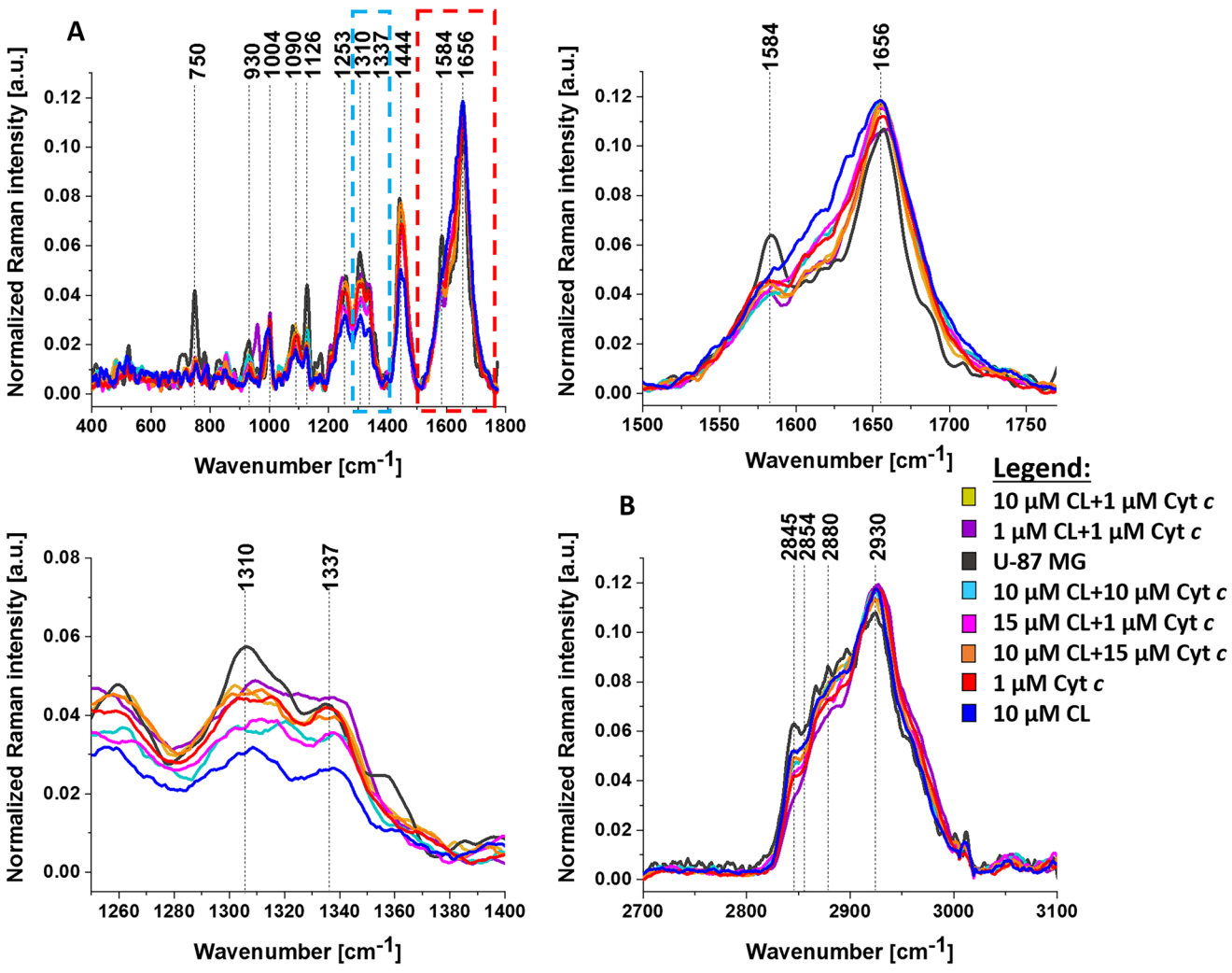

Fig. 4 The average Raman spectra of the mitochondria region for unsupplemented human brain cell U-87 MG (dark gray line) and for U-87 MG cells supplemented with 10 μM cardiolipin + 1 μM cytochrome *c* (yellow line), 1 μM cardiolipin + 1 μM cytochrome *c* (purple line), 10 μM cardiolipin + 10 μM cytochrome *c* (cyan line), 15 μM cardiolipin + 1 μM cytochrome *c* (rose red line), 10 μM cardiolipin + 15 μM cytochrome *c* (orange line), 1 μM cytochrome *c* (red line), 10 μM cardiolipin (blue line) for the fingerprint region (A) and the high-frequency spectral region (B).

Cyt *c* based on the Raman bands at 750 and 1126 cm^{-1}, characteristic of cytochrome *c* and *b*, 1310 cm^{-1} assigned to *c*-type cytochrome, and 1584 cm^{-1} assigned to cytochrome *c*.

To better visualize the biochemical differences upon supplementation with CL and Cyt *c* we present the column bars of Raman intensity for bands at 750, 1126, 1310, 1337, 1444 and 1584 cm^{-1}. The one-way ANOVA Tukey test has been used to indicate differences between samples. Statistically significant results have been marked with an asterisk. Fig. 5 presents Raman band intensities for selected Raman bands for human brain cancer cells U-87 MG: unsupplemented (dark grey bar), and seven types of U-87 MG cells upon supplementation with cardiolipin and cytochrome *c*: 10 μM CL + 1 μM Cyt *c* (yellow bar), 1 μM CL + 1 μM Cyt *c* (purple bar), 10 μM CL + 10 μM Cyt *c* (cyan bar), 15 μM CL + 1 μM Cyt *c* (rose red bar), 10 μM CL + 15 μM Cyt *c* (orange bar), 1 μM Cyt *c* (red bar), and 10 μM CL (blue bar).

In view of the results shown in Fig. 5, it is evident that the most visible differences in mitochondria between the unsupplemented brain cancer cells and the cells with supplementation are observed for the bands at 750 and 1126 cm^{-1} corresponding to cytochrome *c* and *b*, and 1310 and 1584 cm^{-1} corresponding to cytochrome *c*. Comparing the Raman intensities at 750, 1126, 1310 and 1584 cm^{-1} at different supplementations, one can see that the highest concentration of cytochromes is observed for the unsupplemented U-87 MG cells (dark grey bar). Moreover, one can see from Fig. 5C, D and E that the intensity of bands at 1444, 1310, and 1337 cm^{-1} are the lowest for U-87 MG supplemented with 10 μM cardiolipin (blue bar).

The band at 1444 cm^{-1} represents vibrations of lipids, not cytochrome *c*. The vibration at 1337 cm^{-1} represents a band of the reduced Cyt *b* (ferro- (Fe^{2+}) cytochrome *b*), not Cyt *c*. The band at 1310 cm^{-1} corresponds to *c*-type cytochromes but represents the ν_{21} mode (C_m–H) A_{2g} in contrast to vibrations of pyrrole ring (1126 cm^{-1}) or methine bridge (ν_{19}). Therefore the interactions with CL are different from those of the vibrations of 750, 1126 and 1584 cm^{-1} of Cyt *c*.

To explain the decrease in the Raman signals of cytochromes upon interaction with cardiolipin, let us concentrate on the vibration of cytochrome *c* at 1584 cm^{-1}. The band ν_{19} at 1584 cm^{-1} is primarily due to the methine bridge vibrations *via* the C_α–C_m stretching and C_m–H bending modes in the heme group in cytochrome *c*.[59–61] It has been reported that the ν_{19} vibration is very sensitive to the redox status of the central iron ion in the heme group and can be considered a Raman biomarker[2–5] monitoring the efficiency of the electron transport chain. The electron transport chain together with chemiosmosis determines the rate of oxidative phosphorylation. If cytochrome *c* does not accept and transfer electrons the electron transport chain will stop running, and ATP will no longer be produced by chemiosmosis. Without enough ATP, cells cannot carry out the reactions they need to function and, after a long enough period of time, may even die.

The iron ion in cytochrome *c* in the electron transport chain may be in either the ferrous Fe^{2+} or the ferric Fe^{3+} state. The Raman bands of cytochrome *c* are very sensitive to the oxidation of the iron ion. Recently we showed that the change of the redox status from the oxidized Fe^{3+} to the reduced Fe^{2+} cytochrome *c* increases spectacularly the Raman signal intensity.[4,5] We showed that upon cancer development in tissues (in contrast to *in vitro* cells) the Raman signal at 1584 cm^{-1} of cytochrome *c* increases spectacularly demonstrating a spectacular shift to the reduced Fe^{2+} form.[2–5,62] This shift provides evidence that electrons from cytochrome *c* are not properly transported to complex **IV** and decrease the "fast road" to produce effective respiration *via* oxidative phosphorylation, becoming less efficient.

However, the results for cancerous brain cells from Fig. 5 show that the Raman signals of cytochrome *c* at 750, 1126 and 1584 cm^{-1} decrease, not increase, upon supplementation with cardiolipin. It indicates that alterations in the Raman signals of cytochrome *c* upon interaction with CL in mitochondria cannot be explained by the change of the redox status from oxidized Fe^{3+} to its reduced form Fe^{2+}.

It is interesting to note that in contrast to the vibrations of cytochrome *c* the intensity of the bands at 1310, 1337 and 1444 cm^{-1} are the lowest for U-87 MG supplemented with 10 μM cardiolipin in Fig. 5.

The decrease of the Raman signals of the oxidized Fe^{3+} cytochrome *c* in mitochondria upon interaction with cardiolipin has been explained by the transformation of Fe^{3+} cytochrome *c* into iron-oxo (ferryl) intermediates called compound **I** and compound **II**, which are (unprotonated) Fe^{IV}=O or (protonated) Fe^{IV}-OH species that are formed when the binding of cytochrome *c* to cardiolipin converts it from an electron shuttle in electron transport chain (ETC) into a potent peroxidase. The process of transformation of Cyt *c* from an electron shuttle in ETC into a peroxidase has been described earlier.[63–67]

Representative peroxidases have a five-coordinate heme with a vacant distal coordination site that permits the iron center to interact with H_2O_2. In contrast, native cyt *c* is six-coordinated, as the distal coordination site is occupied by methionine Met80. This transformation is explained by the unfolding of Cyt *c* by electrostatic interactions between negatively charged phosphates on CL and positively charged lysines on Cyt *c*. Cardiolipin-induced modifications remove Met80 from the heme iron and activate the precatalytic native state.[63–67] Cardiolipin/H_2O_2-induced covalent modifications transform Fe^{3+} cytochrome *c* into iron-oxo (ferryl) intermediates Fe^{IV}=O or Fe^{IV}-OH species, which have lower Raman signal intensities.[63–67]

Both redox properties and peroxidase activity of Cyt *c* change upon interaction with CL in the mitochondrial membrane, which diminishes the electron donor/acceptor role and blocks the transfer of electrons between complexes **III** and **IV** of the respiratory chain, resulting in the loss of oxidative phosphorylation (respiration) and ATP synthesis.

On the other hand, the increased Cyt *c* peroxidase activity results in disturbing various biological processes such as signaling and apoptosis. Peroxidases or peroxide reductases are

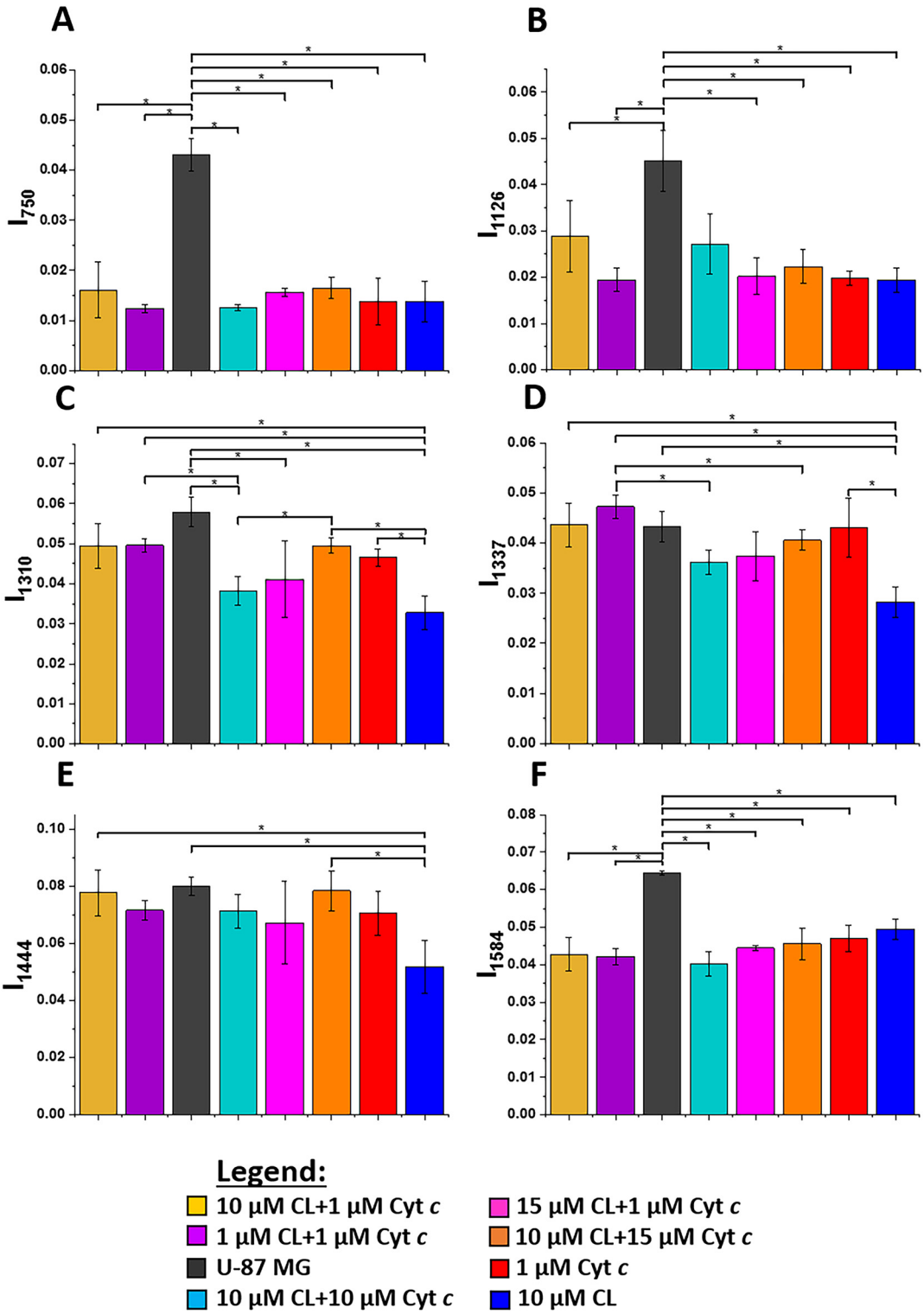

Fig. 5 Histograms represent normalized Raman intensity bands ±SD (SD – standard deviation) calculated for mitochondria region: 750 cm^{-1} (A), 1126 cm^{-1} (B), 1310 cm^{-1} (C), 1337 cm^{-1} (D), 1444 cm^{-1} (E), 1584 cm^{-1} (F) for unsupplemented U-87 MG cells (dark gray) and seven types of supplementation U-87 MG cell lines with cytochrome *c* and cardiolipin: 10 μM cardiolipin + 1 μM cytochrome *c* (yellow), 1 μM cardiolipin + 1 μM cytochrome *c* (purple), 10 μM cardiolipin + 10 μM cytochrome *c* (cyan), 15 μM cardiolipin + 1 μM cytochrome *c* (rose red), 10 μM cardiolipin + 15 μM cytochrome *c* (orange), 1 μM cytochrome *c* (red), 10 μM cardiolipin (blue); the statistically significant results have been marked with asterisk. *; *p*-value ≤ 0.05.

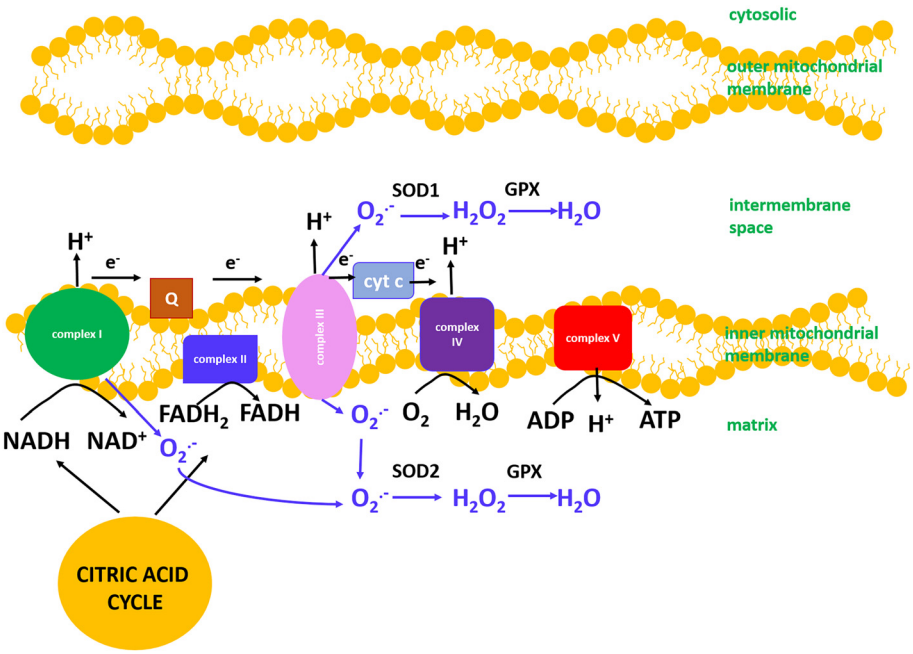

Fig. 6 Mitochondrial electron transport chain and ROS production; SOD – superoxide dismutase; GPX – glutathione peroxidase.

enzymes that break up peroxides, *i.e.*, it catalyzes the oxidation of organic substrates by using hydrogen peroxide, H_2O_2, but other compounds such as lipid peroxides are even more active. Hydrogen peroxide, H_2O_2, produced in mitochondria belongs to mitochondrial reactive oxygen species (mtROS or mROS). The generation of mitochondrial reactive oxygen species mainly takes place at the electron transport chain during the process of oxidative phosphorylation presented in Fig. 6.

The electrons involved in ROS reactions are provided to the ETC in mitochondria from processes occurring in glycolysis and citric acid (TCA) cycle. Glycolysis takes place in the cytoplasm. Within the mitochondrion, the TCA occurs in the mitochondrial matrix, and oxidative metabolism and the electron transport chain occur at the internal mitochondrial membranes. The leakage of electrons at complex **I** and complex **III** from ETC leads to a partial reduction of oxygen to form superoxide. Subsequently, superoxide is quickly dismutated to hydrogen peroxide. Cytochrome *c*–cardiolipin interactions enhance mitochondrial ROS activity because cardiolipin/cytochrome *c* complexes are not effective in scavenging superoxide anions and result in high levels of mitochondrial ROS that activate apoptosis/autophagy pathways capable of inducing cell death.[68–70]

At low levels of CL, Cyt *c* serves as an electron carrier between complex **III** and complex **IV** and allows the mROS products to act as important signaling molecules in regulation and metabolic adaptation as seen in hypoxia[1] or inflammatory response *via* lysophosphatidylcholine and Toll-like receptor 4 and Toll-like receptor 2 bacterial ligands lipopolysaccharide (LPS) and lipopeptides.[68,69] At high levels of CL, the cytochrome *c*/cardiolipin complexes are not effective in scavenging superoxide anions and result in high levels of mitochondrial ROS that activate apoptosis/autophagy pathways capable of inducing cell death.[68–70]

Conclusions

Within the central nervous system (CNS), cardiolipin is found to be an essential player within both neuronal and non-neuronal glial cells, where it regulates metabolic processes, supports mitochondrial functions, and promotes brain cell viability. The cardiolipin–cytochrome *c* interactions can affect the cell's ability to regulate mitochondrial activity. It is now widely accepted that cardiolipin plays a central role in mitochondrial metabolism by maintaining the proper flexibility and morphology of the mitochondrial membranes and by regulating the activity of a variety of enzymes and proteins including cytochrome *c* involved in mitochondrial function. However, the mechanisms are still not well understood. Understanding the underlying regulatory mechanisms requires pathway-targeted, informative experimental data. However, practical experimental design approaches are still in their infancy. Here, we propose an experimental framework by Raman imaging and a model for the identification of regulatory mechanisms in cancers induced by cardiolipin.

We studied the role of cardiolipin–cytochrome *c* interactions in cells' mitochondria by Raman imaging of brain cancer (U-87 MG) cells. This paper provides evidence that cardiolipin–cytochrome *c* interactions are key to mitochondrial energy homeostasis by controlling the redox status of cytochrome *c* in the electron transport chain, switching on/off Fe^{2+}/Fe^{3+} of cytochrome *c* in the electron transport chain and turning on the peroxidase activity. The decrease of the Raman

signals of the oxidized Fe^{3+} cytochrome *c* in mitochondria in a cancer cell upon interactions with cardiolipin suggests the transformation into iron-oxo (ferryl) intermediates called compound **I** and compound **II**, which are (unprotonated) Fe^{IV}=O or (protonated) Fe^{IV}–OH. These species are formed when the binding of cytochrome *c* to cardiolipin converts it from an electron shuttle carrier in the electron transport chain into a peroxidase complex that catalyzes cardiolipin oxidation; this process plays a pivotal role in the mitochondrial stage of oxidative phosphorylation (respiration) and the execution of the cell death program *via* apoptosis. Furthermore, cardiolipin/cytochrome *c* complexes that transform heme centers into ferryl intermediates are not effective in scavenging superoxide anions. This results in the production of high-concentration mROS species. Finally, high levels of mitochondrial ROS activate apoptosis/autophagy pathways capable of inducing cancer development.

The newly discovered role of cytochrome *c* in the electron transport chain, apoptosis and ROS activity will allow the exploitation of this knowledge for drug discovery purposes based on their ability to manipulate cardiolipin peroxidation in cytochrome *c*/cardiolipin complexes.

Data availability statement

The raw data underlying the results presented in the study are available from Lodz University of Technology Institutional Data Access for researchers who meet the criteria for access to confidential data. The data contain potentially sensitive information. Request for access to those data should be addressed to the corresponding author. Data requests might be sent by email to the secretary of the Institute of Applied Radiation Chemistry: w3i34@adm.p.lodz.pl.

Author contributions

Conceptualization: M. K. and H. A.; funding acquisition: H. A.; investigation: M. K. and A. B-D.; methodology: M. K. and A. B-D.; sample preparation: M. K. and K. J.; writing – original draft: M. K. and H. A.; manuscript reviewing: M. K., A. B-D., M. B., and H. A.; supervision: M. B. and H. A.; all authors have read and agreed to the published version of the manuscript.

Conflicts of interest

The authors declare no conflict of interest.

Acknowledgements

This work was supported by the National Science Centre of Poland (Narodowe Centrum Nauki, UMO-2021/43/B/ST4/01547).

References

1 V. E. Kagan, H. A. Bayir, N. A. Belikova, O. Kapralov, Y. Y. Tyurina, V. A. Tyurin, *et al.*, Cytochrome c/cardiolipin relations in mitochondria: a kiss of death, *Free Radicals Biol. Med.*, 2009, **46**(11), 1439–1453.

2 H. Abramczyk, M. K. Brożek-Płuska and M. Kopeć, Double face of cytochrome c in cancers by Raman imaging, *Sci. Rep.*, 2022, 1–11, DOI: **10.1038/s41598-022-04803-0**.

3 H. Abramczyk, J. M. Surmacki, B. Brozek-Pluska and M. Kopec, Revision of Commonly Accepted Warburg Mechanism of Cancer Development: Redox-Sensitive Mitochondrial Cytochromes in Breast and Brain Cancers by Raman Imaging, *Cancers*, 2021, **13**(11), 2599.

4 H. Abramczyk, J. M. Surmacki and B. Brozek-Pluska, Redox state changes of mitochondrial cytochromes in brain and breast cancers by Raman spectroscopy and imaging, *J. Mol. Struct.*, 2022, **1252**, 132134, DOI: **10.1016/j.molstruc.2021.132134**.

5 H. Abramczyk, B. Brozek-Pluska, M. Kopec, J. Surmacki, M. Błaszczyk and M. Radek, Redox imbalance and biochemical changes in cancer by probing redox-sensitive mitochondrial cytochromes in label-free visible resonance raman imaging, *Cancers*, 2021, **13**(5), 960.

6 L. W. Thomas and M. Ashcroft, The Contextual Essentiality of Mitochondrial Genes in Cancer, *Front. Cell Dev. Biol.*, 2021, **9**, 1–7.

7 Y. Fu, T. Zou, X. Shen, P. J. Nelson, J. Li, C. Wu, *et al.*, Lipid metabolism in cancer progression and therapeutic strategies, *MedComm*, 2021, **2**(1), 27–59. Available from: **https://onlinelibrary.wiley.com/doi/abs/10.1002/mco2.27**.

8 M. Pizzuto and P. Pelegrin, Cardiolipin in Immune Signaling and Cell Death, *Trends Cell Biol.*, 2020, **30**(11), 892–903, DOI: **10.1016/j.tcb.2020.09.004**.

9 G. Paradies, V. Paradies, F. M. Ruggiero and G. Petrosillo, Role of cardiolipin in mitochondrial function and dynamics in health and disease: Molecular and pharmacological aspects, *Cells*, 2019, **8**(7), 728, DOI: **10.3390/cells8070728**.

10 A. J. Chicco and G. C. Sparagna, Role of cardiolipin alterations in mitochondrial dysfunction and disease, *Am. J. Physiol.: Cell Physiol.*, 2007, **292**(1), C33–C44, DOI: **10.1152/ajpcell.00243.2006**.

11 S. Ghosh, W. B. Ball, T. R. Madaris, S. Srikantan, M. Madesh, V. K. Mootha, *et al.*, An essential role for cardiolipin in the stability and function of the mitochondrial calcium uniporter, *Proc. Natl. Acad. Sci. U. S. A.*, 2020, **117**(28), 16383–16390.

12 Y. A. Vladimirov, C. Sarisozen, G. K. Vladimirov, N. Filipczak, A. M. Polimova and V. P. Torchilin, The Cytotoxic Action of Cytochrome C/Cardiolipin Nanocomplex (Cyt-CL) on Cancer Cells in Culture, *Pharm. Res.*, 2017, **34**(6), 1264–1275.

13 M. Ren, C. K. L. Phoon and M. Schlame, Metabolism and function of mitochondrial cardiolipin, *Prog. Lipid Res.*, 2014, **55**, 1–16.

14 B. Mohr, K. Shmilovich, I. S. Kleinwächter, D. Schneider, A. L. Ferguson and T. Bereau, Data-driven discovery of cardiolipin-selective small molecules by computational active learning, *Chem. Sci.*, 2022, 4498–4511.
15 S. T. Ahmadpour, K. Mahéo, S. Servais, L. Brisson and J. F. Dumas, Cardiolipin, the mitochondrial signature lipid: Implication in cancer, *Int. J. Mol. Sci.*, 2020, **21**(21), 1–16.
16 M. C. Pangborn, A New Serologically Active Phospholipid from Beef Heart, *Proc. Soc. Exp. Biol. Med.*, 1941, **48**(2), 484–486.
17 M. C. Pangborn, A simplified preparation of cardiolipin with a note on purification of lecithin for serologic use, *J. Biol. Chem.*, 1945, **161**(1), 71–82. Available from: **https://www.sciencedirect.com/science/article/pii/S0021925817415237**.
18 M. Falabella, H. J. Vernon, M. G. Hanna, S. M. Claypool and R. D. S. Pitceathly, Cardiolipin, Mitochondria, and Neurological Disease, *Trends Endocrinol. Metab.*, 2021, **32**(4), 224–237.
19 L. S. Thorne, G. Rochford, T. D. Williams, A. D. Southam, G. Rodriguez-Blanco, W. B. Dunn, *et al.*, Cytoglobin protects cancer cells from apoptosis by regulation of mitochondrial cardiolipin, *Sci. Rep.*, 2021, **11**(1), 1–16, DOI: **10.1038/s41598-020-79830-w**.
20 S. M. Claypool and C. M. Koehler, The complexity of cardiolipin in health and disease, *Trends Biochem. Sci.*, 2012, **37**(1), 32–41, DOI: **10.1016/j.tibs.2011.09.003**.
21 A. Musatov and E. Sedlák, Role of cardiolipin in stability of integral membrane proteins, *Biochimie*, 2017, **142**, 102–111.
22 H. Zhong, M. Xiao, K. Zarkovic, M. Zhu, R. Sa, J. Lu, *et al.*, Mitochondrial control of apoptosis through modulation of cardiolipin oxidation in hepatocellular carcinoma: A novel link between oxidative stress and cancer, *Free Radicals Biol. Med.*, 2017, **102**, 67–76. Available from: **https://www.sciencedirect.com/science/article/pii/S0891584916309790**.
23 A. Sapandowski, M. Stope, K. Evert, M. Evert, U. Zimmermann, D. Peter, *et al.*, Cardiolipin composition correlates with prostate cancer cell proliferation, *Mol. Cell. Biochem.*, 2015, **410**(1–2), 175–185.
24 M. Ott, B. Zhivotovsky and S. Orrenius, Role of cardiolipin in cytochrome c release from mitochondria, *Cell Death Differ.*, 2007, **14**(7), 1243–1247.
25 Y.-J. Chao, J.-F. Chan and Y.-H. H. Hsu, Chemotherapy Drug Induced Discoordination of Mitochondrial Life Cycle Detected by Cardiolipin Fluctuation, *PLoS One*, 2016, **11**(9), 1–17, DOI: **10.1371/journal.pone.0162457**.
26 N. Ikon and R. O. Ryan, Cardiolipin and mitochondrial cristae organization, *Biochim. Biophys. Acta, Biomembr.*, 2017, **1859**(6), 1156–1163, DOI: **10.1016/j.bbamem.2017.03.013**.
27 J. S. Bautista, M. Falabella, P. J. Flannery, M. G. Hanna, S. J. R. Heales, S. A. S. Pope, *et al.*, Advances in methods to analyse cardiolipin and their clinical applications, *TrAC, Trends Anal. Chem.*, 2022, **157**, 116808, DOI: **10.1016/j.trac.2022.116808**.
28 L. Potze, S. Di Franco, C. Grandela, M. L. Pras-Raves, D. I. Picavet, H. A. Van Veen, *et al.*, Betulinic acid induces a novel cell death pathway that depends on cardiolipin modification, *Oncogene*, 2016, **35**(4), 427–437, DOI: **10.1038/onc.2015.102**.
29 D. Jia, J. Zhang, J. Nie, J. P. Andersen, S. Rendon, Y. Zheng, *et al.*, Cardiolipin remodeling by ALCAT1 links hypoxia to coronary artery disease by promoting mitochondrial dysfunction, *Mol. Ther.*, 2021, **29**(12), 3498–3511, DOI: **10.1016/j.ymthe.2021.06.007**.
30 Y. L. Tsang, C. L. Kao, S. C. A. Lin and C. J. Li, Mitochondrial Dysfunction and Oxidative Stress in Aging and Disease, *Biomedicines*, 2022, **10**(11), 2872, DOI: **10.3390/biomedicines10112872**.
31 M. H. McNeely, Cardiolipin Profiling in Metastatic Breast Cancer Cells, *Honors Theses*, 2018, 690.
32 S. Hardy, W. El-Assaad, E. Przybytkowski, E. Joly, M. Prentki and Y. Langelier, Saturated fatty acid-induced apoptosis in MDA-MB-231 breast cancer cells. A role for cardiolipin, *J. Biol. Chem.*, 2003, **278**(34), 31861–31870. Available from: **https://europepmc.org/abstract/MED/12805375**.
33 J. Zhang, W. Yu, S. W. Ryu, J. Q. Lin, G. Buentello, R. Tibshirani, *et al.*, Cardiolipins Are Biomarkers of Mitochondria-Rich Thyroid Oncocytic Tumors, *Cancer Res.*, 2016, **76**(22), 6588–6597.
34 R. J. DeHoog, J. Zhang, E. Alore, J. Q. Lin, W. Yu, S. Woody, *et al.*, Preoperative metabolic classification of thyroid nodules using mass spectrometry imaging of fine-needle aspiration biopsies, *Proc. Natl. Acad. Sci. U. S. A.*, 2019, **116**(43), 21401–21408.
35 M. A. Kiebish, X. Han, H. Cheng, J. H. Chuang and T. N. Seyfried, Cardiolipin and electron transport chain abnormalities in mouse brain tumor mitochondria: Lipidomic evidence supporting the Warburg theory of cancer, *J. Lipid Res.*, 2008, **49**(12), 2545–2556.
36 M. A. Kiebish, X. Han, H. Cheng, A. Lunceford, C. F. Clarke, H. Moon, *et al.*, Lipidomic analysis and electron transport chain activities in C57BL/6J mouse brain mitochondria, *J. Neurochem.*, 2008, **106**(1), 299–312.
37 H. Cheng, D. J. Mancuso, X. Jiang, S. Guan, J. Yang, K. Yang, *et al.*, Shotgun lipidomics reveals the temporally dependent, highly diversified cardiolipin profile in the mammalian brain: Temporally coordinated postnatal diversification of cardiolipin molecular species with neuronal remodeling, *Biochemistry*, 2008, **47**(21), 5869–5880.
38 M. A. Parker, V. King and K. P. Howard, Nuclear magnetic resonance study of doxorubicin binding to cardiolipin containing magnetically oriented phospholipid bilayers, *Biochim. Biophys. Acta, Biomembr.*, 2001, **1514**(2), 206–216.
39 M.G. Fernandez, L. Troiano, L. Moretti, M. Nasi, M. Pinti, S. Salvioli, *et al.*, Early changes in intramitochondrial cardiolipin distribution during apoptosis, *Cell Growth Differ.*, 2002, **13**(9), 449–455.
40 M. Okada, N. I. Smith, A. F. Palonpon, H. Endo, S. Kawata, M. Sodeoka, *et al.*, Label-free Raman observation of cytochrome c dynamics during apoptosis, *Proc. Natl. Acad. Sci. U. S. A.*, 2012, **109**(1), 28–32.

41 J. Zhang, W. Ge and Q. Yu, Structural evaluation of cytochrome c by Raman spectroscopy and its relationship with apoptosis and protein degradation in postmortem bovine muscle, *Food Chem.*, 2021, **362**, 130189.
42 T. Takahashi and T. Ogura, Resonance Raman Spectra of Cytochrome c Oxidase in Whole Mitochondria, *Bull. Chem. Soc. Jpn.*, 2002, **75**(5), 1001–1004, DOI: **10.1246/bcsj.75.1001**.
43 S. Hu, T. G. Spiro, I. K. Morris, J. P. Singh and K. M. Smith, Complete Assignment of Cytochrome c Resonance Raman Spectra via Enzymatic Reconstitution with Isotopically Labeled Hemes, *J. Am. Chem. Soc.*, 1993, **115**(26), 12446–12458.
44 E. Bik, L. Mateuszuk, M. Stojak, S. Chlopicki, M. Baranska and K. Majzner, Menadione-induced endothelial inflammation detected by Raman spectroscopy, *Biochim. Biophys. Acta, Mol. Cell Res.*, 2021, **1868**(2), 118911, DOI: **10.1016/j.bbamcr.2020.118911**.
45 B. Milorey, D. Malyshka and R. Schweitzer-Stenner, pH Dependence of Ferricytochrome c Conformational Transitions during Binding to Cardiolipin Membranes: Evidence for Histidine as the Distal Ligand at Neutral pH, *J. Phys. Chem. Lett.*, 2017, **8**(9), 1993–1998.
46 R. V. Chertkova, A. M. Firsov, N. A. Brazhe, E. I. Nikelshparg, Z. V. Bochkova, T. V. Bryantseva, *et al.*, Multiple Mutations in the Non-Ordered Red Ω-Loop Enhance the Membrane-Permeabilizing and Peroxidase-like Activity of Cytochrome c, *Biomolecules*, 2022, **12**(5), 1–15.
47 J. Hanske, J. R. Toffey, A. M. Morenz, A. J. Bonilla, K. H. Schiavoni and E. V. Pletneva, Conformational properties of cardiolipin-bound cytochrome c, *Proc. Natl. Acad. Sci. U. S. A.*, 2012, **109**(1), 125–130.
48 N. A. Brazhe, M. Treiman, A. R. Brazhe, N. L. Find, G. V. Maksimov and O. V. Sosnovtseva, Mapping of Redox State of Mitochondrial Cytochromes in Live Cardiomyocytes Using Raman Microspectroscopy, *PLoS One*, 2012, **7**(9), 1–8.
49 H. Salehi, E. Middendorp, I. Panayotov, P.-Y. C. Dutilleul, A.-G. Vegh, S. Ramakrishnan, *et al.*, Confocal Raman data analysis enables identifying apoptosis of MCF-7 cells caused by anticancer drug paclitaxel, *J. Biomed. Opt.*, 2013, **18**(5), 056010.
50 Y. Sun, S. Ge, J. Xue, X. Zhou, W. Lu, G. Li, *et al.*, Highly sensitive detection of cytochrome c in the NSCLC serum using a hydrophobic paper based–gold nanourchin substrate, *Biomed. Opt. Express*, 2020, **11**(12), 7062.
51 J. Muenzner, J. R. Toffey, Y. Hong and E. V. Pletneva, Becoming a peroxidase: cardiolipin-induced unfolding of cytochrome c, *J. Phys. Chem. B*, 2013, **117**(42), 12878–12886.
52 G. K. Vladimirov, A. S. Vikulina, D. Volodkin and Y. A. Vladimirov, Structure of the complex of cytochrome c with cardiolipin in non-polar environment, *Chem. Phys. Lipids*, 2018, **214**, 35–45.
53 Y. A. Vladimirov, E. V. Proskurnina and A. V. Alekseev, Molecular mechanisms of apoptosis. Structure of cytochrome c-cardiolipin complex, *Biochem*, 2013, **78**(10), 1086–1097.
54 A. V. Birk, W. M. Chao, C. Bracken, J. D. Warren and H. H. Szeto, Targeting mitochondrial cardiolipin and the cytochrome c/cardiolipin complex to promote electron transport and optimize mitochondrial ATP synthesis, *Br. J. Pharmacol.*, 2014, **171**(8), 2017–2028.
55 J. P. Kitt, D. A. Bryce, S. D. Minteer and J. M. Harris, Raman Spectroscopy Reveals Selective Interactions of Cytochrome c with Cardiolipin That Correlate with Membrane Permeability, *J. Am. Chem. Soc.*, 2017, **139**(10), 3851–3860.
56 S. C. Sun, H. W. Huang, Y. T. Lo, M. C. Chuang and Y. H. H. Hsu, Unraveling cardiolipin-induced conformational change of cytochrome c through H/D exchange mass spectrometry and quartz crystal microbalance, *Sci. Rep.*, 2021, **11**(1), 1–11, DOI: **10.1038/s41598-020-79905-8**.
57 M. Kopeć, K. Beton and K. A. H. Jarczewska, Hyperglycemia and cancer in human lung carcinoma by means of Raman spectroscopy and imaging, *Sci. Rep.*, 2022, **12**, 18561. Available from: **https://www.biorxiv.org/content/10.1101/2022.04.05.487128v1%0A**, **https://www.biorxiv.org/content/10.1101/2022.04.05.487128v1.abstract**.
58 T. C. Strekas and T. G. Spiro, Cytochrome c: Resonance Raman spectra, *Biochim. Biophys. Acta, Protein Struct.*, 1972, **278**(1), 188–192. Available from: **https://www.sciencedirect.com/science/article/pii/0005279572901213**.
59 T. G. Spiro and T. C. Strekas, Resonance Raman Spectra of Heme Proteins. Effects of Oxidation and Spin State, *J. Am. Chem. Soc.*, 1974, **96**(2), 338–345.
60 M. Abe, T. Kitagawa and Y. Kyogoku, Resonance Raman spectra of octaethylporphyrinato-Ni(II) and meso-deuterated and ^{15}N substituted derivatives. II. A normal coordinate analysis, *J. Chem. Phys*, 1978, **69**, 4526–4534.
61 S. Hu, K. M. Smith and T. G. Spiro, Assignment of protoheme Resonance Raman spectrum by heme labeling in myoglobin, *J. Am. Chem. Soc.*, 1996, **118**(50), 12638–12646.
62 H. Abramczyk, A. Imiela and J. Surmacki, Novel strategies of Raman imaging for monitoring intracellular retinoid metabolism in cancer cells, *J. Mol. Liq.*, 2021, **334**, 116033, DOI: **10.1016/j.molliq.2021.116033**.
63 L. V. Basova, I. V. Kurnikov, L. Wang, V. B. Ritov, N. A. Belikova, I. I. Vlasova, *et al.*, Cardiolipin switch in mitochondria: Shutting off the reduction of cytochrome c and turning on the peroxidase activity, *Biochemistry*, 2007, **46**(11), 3423–3434.
64 M. Li, W. Sun, V. A. Tyurin, M. DeLucia, J. Ahn, V. E. Kagan, *et al.*, Activation of Cytochrome C Peroxidase Function Through Coordinated Foldon Loop Dynamics upon Interaction with Anionic Lipids, *J. Mol. Biol.*, 2021, **433**(15), 167057. Available from: **https://www.sciencedirect.com/science/article/pii/S0022283621002758**.
65 L. Fiorucci, F. Erba, R. Santucci and F. Sinibaldi, Cytochrome c Interaction with Cardiolipin Plays a Key Role in Cell Apoptosis: Implications for Human Diseases, *Symmetry*, 2022, **14**(4), 1–17.

66 P. C. E. Moody and E. L. Raven, The Nature and Reactivity of Ferryl Heme in Compounds i and II, *Acc. Chem. Res.*, 2018, **51**(2), 427–435.
67 V. Yin, G. S. Shaw and L. Konermann, Cytochrome c as a Peroxidase: Activation of the Precatalytic Native State by H_2O_2-Induced Covalent Modifications, *J. Am. Chem. Soc.*, 2017, **139**(44), 15701–15709.
68 X. Li, P. Fang, Y. Li, Y. M. Kuo, A. J. Andrews, G. Nanayakkara, *et al.*, Mitochondrial reactive oxygen species mediate lysophosphatidylcholine-induced endothelial cell activation, *Arterioscler., Thromb., Vasc. Biol.*, 2016, **36**(6), 1090–1100.
69 A. P. West, I. E. Brodsky, C. Rahner, D. K. Woo, H. Erdjument-Bromage, P. Tempst, *et al.*, TLR signalling augments macrophage bactericidal activity through mitochondrial ROS, *Nature*, 2011, **472**(7344), 476–480.
70 T. Finkel, Signal transduction by mitochondrial oxidants, *J. Biol. Chem.*, 2012, **287**(7), 4434–4440, DOI: **10.1074/jbc.R111.271999**.